Robotica: (2021) volume 39, pp. 1711–1728. © The Author(s), 2021. Published by Cambridge University Press.
doi:10.1017/S0263574720001459

An Identification-Based Method Improving the Transparency of a Robotic Upper Limb Exoskeleton

Dorian Verdel†‡¶*[a], Simon Bastide‡¶[a], Nicolas Vignais‡¶, Olivier Bruneau† and Bastien Berret‡¶§

†*Université Paris-Saclay, ENS Paris-Saclay, LURPA, 94235 Cachan, France*
E-mail: olivier.bruneau@ens-paris-saclay.fr
‡*Université Paris-Saclay, CIAMS, 91405 Orsay, France*
E-mails: simon.bastide@universite-paris-saclay.fr, nicolas.vignais@universite-paris-saclay.fr, bastien.berret@universite-paris-saclay.fr
¶*CIAMS, Université d'Orléans, 45067 Orléans, France*
§*Institut Universitaire de France, Paris, France*

(Accepted December 14, 2020. First published online: February 3, 2021)

SUMMARY
Over the past decade, research on human–robot collaboration has grown exponentially, motivated by appealing applications to improve the daily life of patients/operators. A primary requirement in many applications is to implement highly "transparent" control laws to reduce the robot impact on human movement. This impact may be quantified through relevant motor control indices. In this paper, we show that control laws based on careful identification procedures improve transparency compared to classical closed-loop position control laws. A new performance index based on the ratio between electromyographic activity and limb acceleration is also introduced to assess the quality of human exoskeleton interaction.

KEYWORDS: Control laws; Identification; Human/Robot interaction; Transparency indices; Motor control.

1. Introduction

Over the past decade, exoskeletons encountered a large success, mainly for handling and rehabilitation applications. Exoskeleton-type assistive devices aim at providing efforts to one or several segments in order to assist the user in achieving specifics tasks. Amongst the different types of exoskeletons, active robotic devices are especially promising because they offer a great versatility that cannot be equalled by passive devices. They may be useful to support injured or disabled people in recovering and performing the movements required in daily living activities.[1] They may as well reduce joint efforts and prevent the development of musculoskeletal disorders at work.[2,3] For instance, improvements of rehabilitation protocols were envisioned by using upper limbs powered exoskeletons.[4,5] Benefits in terms of prevention of workers' musculoskeletal disorders[6] and metabolic energy savings[7] could also be expected with this type of powered assistance. However, despite these potential benefits, the concrete usability of powered assistive exoskeletons is hampered by the absence of evidence for *in situ* efficiency. Indeed, meta-analyses do not yet highlight any clear consensus on the positive effects of robot-assisted therapies compared to conventional ones.[8]

[a]These authors contributed equally.

* Corresponding author. E-mail: dorian.verdel@ens-paris-saclay.fr

Furthermore, the possible industrial applications may be challenged by the evidence of an average 30% movement slowdown when wearing a robotic "transparent" exoskeleton (see below) of the upper limb,[9,10] which could result in a critical decrease in productivity. Besides hardware and technical issues, their lack of concrete usability is mainly due to the fact that only few exoskeleton devices allow a symbiotic interaction with humans. Exoskeleton research and development have recently been interested in evaluating exoskeletons from a more human-centred point of view, by taking into account the human response to interaction with an exoskeleton as a critical feature of human/exoskeleton interactions (HEI).[11–17] Indeed, how humans adapt their motor control to the interaction forces induced by wearing a robotic exoskeleton implementing some control laws should drive the development of new and more intuitive control laws.

The ability of an exoskeleton not to change or influence human movement is called transparency.[18] Theoretically, a perfect transparency would be reached if the interaction forces between the exoskeleton and the user are equal to zero. In reality, achieving perfect transparency is impossible, especially because human movements cannot be fully predicted.[19] Getting as close as possible to this situation is desired in many applications[20] as it may improve the quality of the interaction and contribute to better master task-dependent control laws. In general, a transparent exoskeleton should be able to compensate its own weight, friction, inertia and, in the case of load carrying, the weight and inertia of the mass being carried. Alternatively, if a sufficient degree of transparency is not achieved in baseline experiments without loads, an acceptable compensation of interactions with external objects will not be possible and the user will have to manage a combination of flawed compensations of the exoskeleton and of the carried load. In other words, a lack of transparency means that unwanted or uncontrolled interaction forces will appear, which may induce a motor adaptation from the user and/or prevent the acceptability of the device. Therefore, transparency is a primary and crucial step towards both industrial and medical applications in the sense that it provides a baseline setting for more advanced scenarios such as compensation for the weight of the user's arm or any other control law modifying the interaction forces. Overall, we argue that transparency is a necessary condition towards more symbiotic HEI.

2. State of the Art

2.1. Assess and improve transparency

The assessment of transparency has generally been done by comparing movement indices under natural conditions (without wearing exoskeletons) and while wearing the exoskeleton.[10,21] Often, these studies have focused on movements involving many degrees of freedom such as pointing movements performed with the whole upper limb thereby making it difficult to understand non-linear phenomena that may occur during the interaction in such complex movements. Moreover, this approach tends to contrast with an important part of the literature on human motor control, which has largely focused on simpler movements involving one[22,23] or two degrees of freedom.[24,25] Human motor control studies have often focused on simple movements because of the variability that can appear between subjects when achieving complex movements. This variability makes the derivation of explanatory models far more complicated. Moreover, the interpretation of physiological measures for complex movements, such as electromyographic (EMG) signals, can be very challenging. As our objective is to design new control laws that impact as little as possible the human motor control (i.e., that maximise transparency), it appears relevant to investigate their effects on well-known and widely documented human movements. Therefore, our approach is to reduce the complexity of the studied movement to a simple movement involving only one degree of freedom to carefully assess the quality of different transparent control laws.

Traditional methods employed to improve transparency have primarily focused on the mechanical design of exoskeletons' joints[26,27] and connections with the user. Indeed, the system $\{human + exoskeleton\}$ is highly hyperstatic with simple connections and therefore implies unwanted interaction forces. Transparency and comfort have been improved by adding passive degrees of freedom, that release hyperstatic constraints, in the connections' design.[14,28,29] Furthermore, approaches based on human movement prediction are promising for previously known[19] or repetitive movements,[30] but their extension to a wider range of behaviours is still a challenge due to the difficulty of predicting the user's intended movement in general settings. In

https://doi.org/10.1017/S0263574720001459 Published online by Cambridge University Press

another approach, the use of force sensors could be relevant to allow the exoskeleton to follow the user's movements by directly minimising the interaction forces.[19,31] Nevertheless, this method is not often used because few exoskeletons include force sensors as standard equipment. More often, the robot's control is based on a closed-loop position control[1,9,19,21] as most robotic devices use incremental encoders as on-board sensors. Thus, the most direct solution for a better transparency appears to be controlling the robot so that it compensates its own dynamics. To make this solution reliable, a coherent model of the robot has to be designed and its parameters have to be known as precisely as possible. Yet, few studies addressed the role of identification to improve exoskeletons' transparency.

Our premise is that an accurate identification of the robot, possibly introducing direction-dependent models, may improve transparency. Indeed, direction-dependent models allow to take into account phenomena that are not described by classical rigid body dynamics.[32] Nevertheless, this type of model is very rarely studied in the literature. This approach is quite different, but complementary, from current methods adopted in the literature such as identifying the parameters of the interaction between humans and robots instead of identifying the robot itself.[33]

2.2. Identification methodologies

Identification is a large field of robotics that has been extensively studied over the past decades. A great variety of models and experiments can be used in order to identify a robot, but all of them can be classified into one of the two methods, direct identification of all parameters or step-by-step identification of groups of parameters.[34] Then, two approaches co-exist, one non-parametric and one parametric.[35,36] The first approach consists in considering the system as a black box following a general structure to identify, such as the general linear model structure.[36,37] One of the limitations of this approach is the lack of interpretation that can be made after the identification, which is why the present study is not based on it. The second approach consists in identifying a model arising from classical mechanical models such as direct or inverse geometrical models to improve the robot positioning.[38–40] Currently, identifications often need to describe the dynamics of robots, therefore Newton's equations are often a basis for identification models.[41,42] The main limit of this approach is that in order to take into account all the possible phenomena, the number and observability of parameters can be an issue. Nevertheless, as our study focuses on one degree of freedom, this approach is the one retained in the present study. Newton's equations involve mainly consensual physical interactions and parameters (inertia, Coriolis effect,...), but most of the the time friction is taken into account to model robots. The models used to describe friction are far more diverse and directly depend on the application.[43] The most widely spread model is a non-linear model combining a Coulomb dry friction and a viscous friction proportional to velocity.[19,41,44,45] This model is simple and involves very few parameters, however, it can be inaccurate in certain applications. More complex models, dependent on the load, the sign of velocity and the output power have then been developed.[32] These dependencies can, for instance, capture the changes of contact surfaces and loads in the transmission when the sign of the power changes. The drawback is that such models involve more parameters and are, consequently, more difficult to identify. Nevertheless, they can be better suited when working with systems that are highly backdriveable and flexible. As presented in the next section, the exoskeleton used in the present study belongs to this category, therefore, models taking into account unusual dependencies such as the sign of velocity are potentially relevant to model it accurately.

The rest of this paper is hence organised as follows: In Section 3, the identification methodology, adapted to the characteristics of the ABLE upper limb exoskeleton,[27] is outlined and the obtained results are analysed. Then, in Section 4, the experimental protocol testing the influence of the proposed control laws on human motor control is described and a new performance index based on EMG signals and accelerations is introduced. Finally, the results of these experimental tests are exposed and discussed in Section 5.

3. Identification

3.1. Presentation of ABLE

This study is conducted on an ABLE upper limb exoskeleton (see Fig. 1) with four actuated joints and one free translation that cannot be directly monitored (in terms of position and velocity).

https://doi.org/10.1017/S0263574720001459 Published online by Cambridge University Press

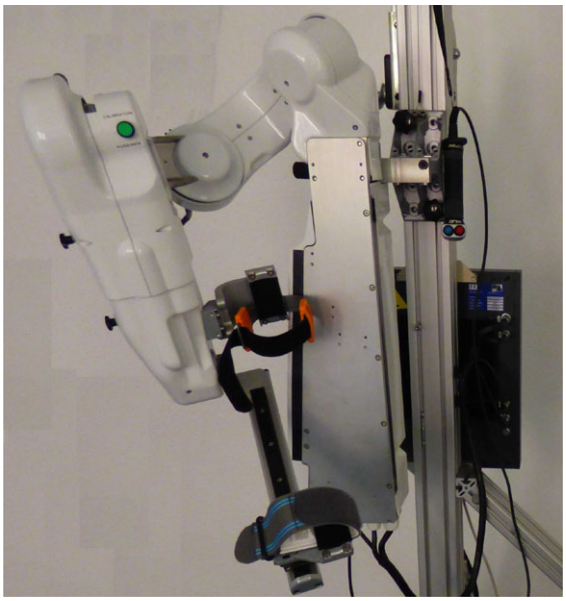

Fig. 1. Picture of the 4D ABLE exoskeleton used in this study.

These four actuated joints correspond to the three rotations of the human shoulder (internal/external rotation, flexion/extension and abduction/adduction) and to the rotation of the human elbow (flexion/extension). The free joint is the last one of the chain and takes the form of a slider (i.e., a prismatic joint) moving on a rail to adapt the distance between the robot elbow and the human wrist during the movement. The presence of this joint is motivated by ergonomic considerations. The release of translations along the main axis of the limb segment prevents the development of a hyperstatic force.[14] This robot has promising capacities in terms of transparency[26,27] because of high levels of backdriveability. Nevertheless, these high levels of backdriveability can lead to complex processes of identification of the dynamics of the robot, starting with friction.

3.2. Geometric and dynamic models

The need for high levels of transparency implies, in our approach, a high quality of identification of the dynamic parameters of the robot. The objective is to provide an accurate compensation of the robot's dynamics. Nevertheless, this step is often neglected to the benefit of a closed-loop "black box" control.

General dynamic approach. In ABLE's case, the transmission is designed to be particularly compliant[26] and, therefore introduces a lot of flexibilities and assembly gaps that generate a lot of friction differences between the different directions of movement. As described in Section 2.2, a lot of friction models already exist in the literature. In particular, the model developed in ref. [32] seems adapted to our situation as it takes into account the sign of the output power and the load. Nevertheless, this model is particularly complex to identify as its identification requires multiple pre-identified external payloads and many trials. In order to limit the number of different coefficients to identify, and therefore improve their observability, and to limit the number of trials, a differentiated identification is performed for upward and downward movements. Finally, the classical model $\tau_f = sign(\dot{q})\tau_C + \nu\dot{q}$ and its static part expressed as $\tau_f = \tau_{adh}$, are used for this study because of their limited number of coefficients. As this model does not take into account all dependencies of friction in ABLE, differences of identification between upward and downward movements will be accounted for by the other coefficients, such as the gravitational torque as described in Section 3.4.

Dynamical effects other than friction also affect the transparency, particularly the gravity-related efforts and the inertia of the system. Therefore, the generic dynamic model[45] presented in Eq. (1) is identified by considering two sets of the parameters, based on the sign of the velocity, as described previously:

$$\mathcal{M}(\mathbf{q})\ddot{\mathbf{q}} + \mathcal{C}(\mathbf{q}, \dot{\mathbf{q}}) + \mathcal{G}(\mathbf{q}) + sign(\dot{\mathbf{q}})\tau_C + \nu\dot{\mathbf{q}} = \tau_{\mathbf{m}}, \quad (1)$$

https://doi.org/10.1017/S0263574720001459 Published online by Cambridge University Press

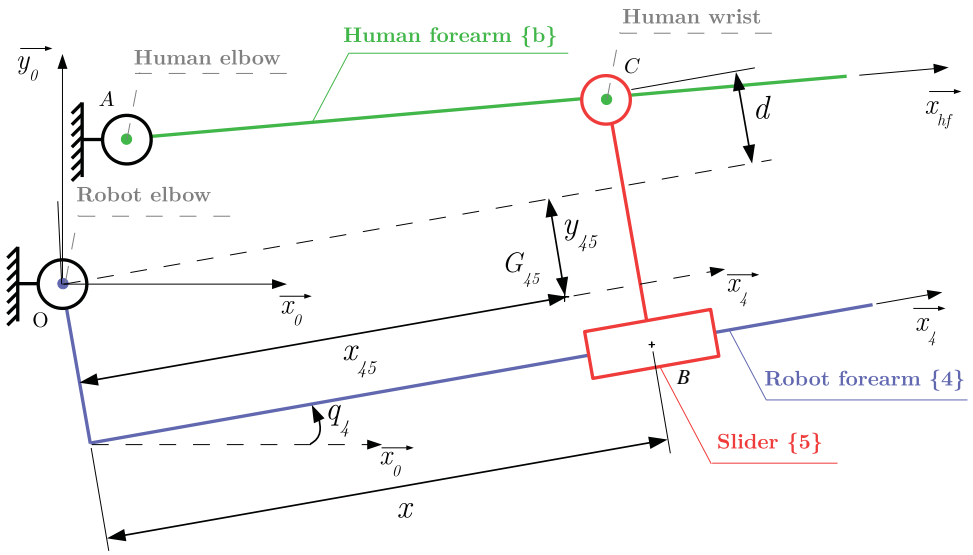

Fig. 2. Kinematic model of the last axis of ABLE with human forearm.

where $\mathcal{M}(\mathbf{q})$ is the inertia matrix, $\mathcal{C}(\mathbf{q}, \dot{\mathbf{q}})$ is the vector containing the Coriolis/centripetal terms, $\mathcal{G}(\mathbf{q})$ is the vector containing the gravitational torques, τ_C is the Coulomb dry friction torque, ν is the viscous friction coefficient, $\tau_{\mathbf{m}}$ is the actuators torques vector, $\ddot{\mathbf{q}}$ is the joint accelerations vector, $\dot{\mathbf{q}}$ is the joint velocities vector and $\mathbf{q}$ is the joint positions vector.

As a conclusion, our approach is a new hybrid approach between a non-parametric identification and a parametric identification (see Section 2.2) in the sense that the values held by the identified coefficients are not the "real values" but the form of the model itself arises from Newton's equations.

Identification restrictions. In agreement with previous motor control studies, human elbow flexion/extension movements are of special interest in the present study (see Section 2.1 for the rationale). As a consequence, we shall focus on the identification of the model of ABLE's elbow, which is dependent on the position x of the slider {5} (see Fig. 2). The position of this slider is the main identification problem regarding the present ABLE exoskeleton. As this position is not measurable by internal means, an external measure is needed. The coupled kinematic model integrating both human upper limb and ABLE is presented in Fig. 2.

In this model, G_{45} is the centre of gravity of the group $\{4 + 5\}$. This kinematic model is used to write two models, a geometric model that is used to estimate the position of the point C in the frame $(O, \overrightarrow{x_4}, \overrightarrow{y_4})$, which is the robot frame, and a dynamic model that contains all parameters influencing the transparency as described in Section 3.1. The geometric model is written in Eq. (2); the two parameters of this model (x and d) should be identified to estimate the position of the slider:

$$\begin{cases} X = x\cos(q_4) - d\sin(q_4) \\ Y = x\sin(q_4) + d\cos(q_4), \end{cases} \tag{2}$$

where X and Y are the coordinates of the point C in the frame $(O, \overrightarrow{x_0}, \overrightarrow{y_0})$, which is the opto-electronic system frame of reference translated to the point O and q_4 is the angular ABLE's elbow position.

The dynamic model derived from Eq. (1) and Fig. 2 is written as in Eq. (3) to describe the behaviour of ABLE's last actuated joint:

$$\tau_{m,4} = \left(m_{45}g\,(x_{45}(x)\cos(q_4) + y_{45}(x)\sin(q_4)) + \nu_4\dot{q_4} + J_{eq}(x)\ddot{q_4} + sign(\dot{q_4})\tau_{dry,4}\right)\frac{1}{r_4}, \tag{3}$$

where $\tau_{m,4} = k_t i_4$ is the torque of the fourth motor estimated with the motor current i_4 and the motor constant k_t. The first parameters that must be identified are $m_{45}x_{45}(x)$ and $m_{45}y_{45}(x)$. They will allow to design an accurate gravity compensation taking into account the position of the slider. Then, the following parameters must be identified: $\tau_{dry,4}$ for the Coulomb friction compensation, ν_4 for

https://doi.org/10.1017/S0263574720001459 Published online by Cambridge University Press

the viscous friction compensation and $J_{eq}(x)$, which is the equivalent inertia of segments {4} and {5} at the joint level, for the inertial compensation. Finally, r_4 is the reduction ratio given by the constructor for the last actuated axis. The inertial coefficient $J_{eq}(x)$ is dependent on the slider position by a second degree relation arising from the Huygens theorem. Therefore, this moment of inertia is described by three coefficients, as written in Eq. (4).

$$J_{eq}(x) = a_0 + a_1 x + a_2 x^2. \tag{4}$$

3.3. Identification methodology

The identification methodology that is applied is a step-by-step methodology. The main advantage of this methodology is to ensure the best possible observability of the different parameters on a mono-axis identification by isolating them and identifying them in different trials. This method also allows to work on more configurations of the device than just the classical sinusoidal and trapezoidal motions and, therefore, to describe other possible behaviours. The inconvenient of this type of method is the risk of accumulating errors on each step of identification, therefore multiple identifications of each coefficients are achieved. A three-step protocol is implemented to conduct the identification. The first step of this protocol consists in acquiring current and position measures while holding static positions in order to achieve a first identification of the gravity torque and Coulomb adherence coefficients. The second step is the acquisition of current, position and velocity measures during constant velocities movements in order to identify again the gravity torque model, to minimise errors accumulation, and identify the Coulomb and viscous frictions compensations. Finally, a wave excitation of the last axis is implemented and measured in order to identify the inertial coefficients presented in Eq. (4). Another method, that is not retained in the present study, is to identify all the parameters in one or two trials (as described in Section 2.2). This method gives slightly less accurate results on our robot but reduces drastically the number of trials. As our study focuses on one degree of freedom, the solution giving the better results is retained.

As explained in Section 3.2, the position x of the slider during the trials must be known in order to obtain a fine identification of ABLE. As this position cannot be measured by internal means, an optoelectronic system, composed of eight infrared cameras and 3 mm reflective markers placed on the robot, has been used to estimate it (©Qualisys, Göteborg, Sweden).

The different protocols implemented are described below.

- Static task (position control loop implemented with a Proportional Integral (PI) correction at 1 kHz):
  - Twenty positions distributed equally across the whole angular capacity of the last joint for six different positions of the slider distributed equally along the rail to cover the whole working space.
  - Each position is maintained for 5 s in order to collect large amounts of data and to make sure that the system has reached a stable position.
- Constant velocities and dynamic tasks (velocity control loop implemented with a PI correction at 1 kHz):
  - Five different control velocities distributed equally across the interval [1, 11] (rev/s) and 25 s of sinusoidal wave excitation for the same positions of the slider as in the static experiment.
  - Each constant velocity is used for one upward and one downward movement.

The sinusoidal wave used for the identification of the inertia follows the expression presented in Eq. (5):

$$q_4(t) = A\sin(\omega(t)t)\ , \quad \text{where } \omega(t) = 1 + 3\frac{t}{T}, \tag{5}$$

where the amplitude is $A = 0.5$ rad, the duration is $T = 25$ s and the pulsation $\omega(t)$ is expressed in rad/s.

For all the tasks, the motor current and the angular position of the motor are measured at 1 kHz. Additionally, the angular velocity and acceleration are estimated by numerical differentiation and the position of the slider is estimated thanks to optoelectronic measures (179 Hz). Least squares methods are used to estimate the axis of rotation of the elbow. All the current measures provided by ABLE's

https://doi.org/10.1017/S0263574720001459 Published online by Cambridge University Press

Table I. Statistics on mean absolute error.

Method	Mean	Standard deviation	Min	Median	Max
Without dissociation (A)	0.159	0.0712	0.0713	0.142	0.268
With dissociation (A)	0.0473	0.0252	0.0288	0.0429	0.131

controller and all position measures provided by the optoelectronic system are filtered by a low-pass filter (based on a sliding mean on n values with $n = 100$ for the current measures and $n = 40$ for the position measures). All the estimations of parameters are then performed thanks to the "*lsqnonlin*" function from the *Optimization Toolbox* of ©MATLAB (MathWorks, Natick, MA, USA).

Methodology validation. As described previously, our approach consists in a dissociated identification according to the sign of velocity. This choice is made to simplify the model to identify (and therefore simplify the identification process) while describing accurately the behaviour of the robot. To support this methodology, we conduct an analysis on 18 trials carried out under 3 conditions. The 6 sinusoidal trials and the 6 constant velocities trials previously performed for the identification (see the tasks description above) are used and 6 trials at low constant velocity (10 upward and 10 downward movements each at 1 rev/s) with 6 different positions of the slider are added to the analysis. Then, for each trial, the mean absolute model error is computed without dissociation and with dissociation as presented in Eq. (6),

$$e = \frac{1}{N}\sum_{j=1}^{N} |i_{4,j} - \hat{i}_{4,j}|, \tag{6}$$

where e is the mean absolute model error in amperes, N is the number of measures of the trial, $i_{4,j}$ is the jth measure of the motor current, $\hat{i}_{4,j}$ is the jth estimation of the motor current and "4" is the number of the considered joint (elbow). The estimation of the motor current is obtained with Eq. (3) and measurements of the position, velocity and acceleration of the robot.

After gathering data on these trials, a statistical analysis is conducted. Classical indices are computed and a paired t-test is carried out between the 2 sets of 18 values of the model error (one set with dissociation and one set without). The significance value of the t-test is fixed at $p < 0.05$.

3.4. Results

Validation. As expected given the friction model presented previously,[32] differences appeared between the models identified for upward and downward movements. Due to the choice of model made in Section 3.1, these differences are passed on to all the identified coefficients. Furthermore, an identification based only on one model without dissociation between upward and downward movements would not be satisfying. The results of the methodological validation are presented in Table I.

The result of the comparison of the two sets with a paired t-test shows a significant difference ($t = 5.422$, $p = 4.572 \times 10^{-5}$). A boxplot representing these data and an example of the improvement in the identification accuracy with the direction-dependent identifications are given in Fig. 3.

All these results show that our method greatly improves the accuracy of the identification process. Indeed, overall, the mean model error is approximately divided by a factor 3.4 and the reduction of model error was significant on 18 trials. Moreover, these results show that a classical identification without dependency on movement direction results in a relatively large model error, making a purely compensatory law unreliable. Our method could also be applied with a different approach regarding the step-by-step procedure. Indeed, all coefficients could be identified at once as long as the system is solicited in both movement directions with numerous different velocities and accelerations.

Identified values. All the identification parameters obtained through the previous process are reported into the Table II below.

As it can be seen in Table II, our approach increases the number of parameters compared to a non-dissociated approach. As previously stated, this does not increase the number of trials to achieve the identification. Nevertheless, it does increase the complexity of the implementation because of the

https://doi.org/10.1017/S0263574720001459 Published online by Cambridge University Press

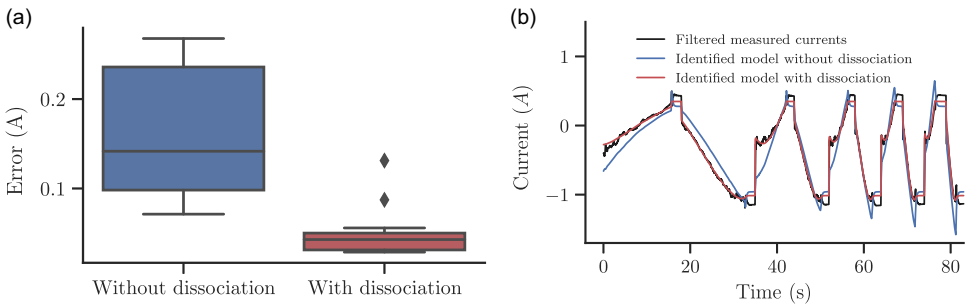

Fig. 3. Results of the validation procedure. (a) Boxplot representing the distribution of errors across trials for both methods. (b) Motor current for a variable velocity command. The red line shows an identification improvement.

Table II. Results obtained through the identification process (x: slider position in m).

Movement direction	$x_{45}m_{45}$ **(m.kg)**	$y_{45}m_{45}$ **(m.kg)**	$\tau_{adh,4}$ **(N.m)**	$\tau_{dry,4}$ **(N.m)**	v_4 **(m.kg/s)**
Downward	$0.98x - 0.45$	-0.13		0.047	0.018
Static	$0.46x - 0.19$	-0.069	-0.12		
Upward	$1.68x - 0.57$	-0.36		0.028	0.0052

Movement direction	a_0 **(kg.m^2)**	a_1 **(kg.m)**	a_2 **(kg)**
Downward	-0.0019	-0.043	-0.081
Static			
Upward	-0.00063	-0.050	-0.096

number of parameters to take into account. For a n-degrees of freedom serial robot with p parameters to identify in each joint (p being the number of parameters with dissociated identification) and by considering coupling between all axes and directions, the total number of parameters to identify would be,

$$N = p \sum_{i=0}^{n-1} 2^i = p(2^n - 1), \tag{7}$$

where N is the total number of parameters and $2^n - 1$ is the number of directional sets to identify. This exponential result seems acceptable for upper limb exoskeletons that often have a maximum of seven degrees of freedom but it may be a limiting factor for whole-body robots where dozens of degrees of freedom are used.

4. Experimental Protocol

4.1. Materials and task

Participants. Six healthy right-handed young adults (*three* females, *three* males, 25 ± 1.3 years, 175.5 ± 5.6 cm height, 63.5 ± 6.1 kg weight) participated in this study. All the participants were naive to the purpose of the experiment. Written informed consent was obtained from each participant as required by Helsinki declaration.[46] The ethical committee for research (Université Paris-Saclay, 2017-34) approved the experimental protocol.

Materials. The experimentations are conducted on the ABLE exoskeleton identified in Section 3. The Qualisys optoelectronic system is used to track the human and robot limbs during movements and therefore to extract the kinematical characteristics of the movement. Reflective markers are placed as

https://doi.org/10.1017/S0263574720001459 Published online by Cambridge University Press

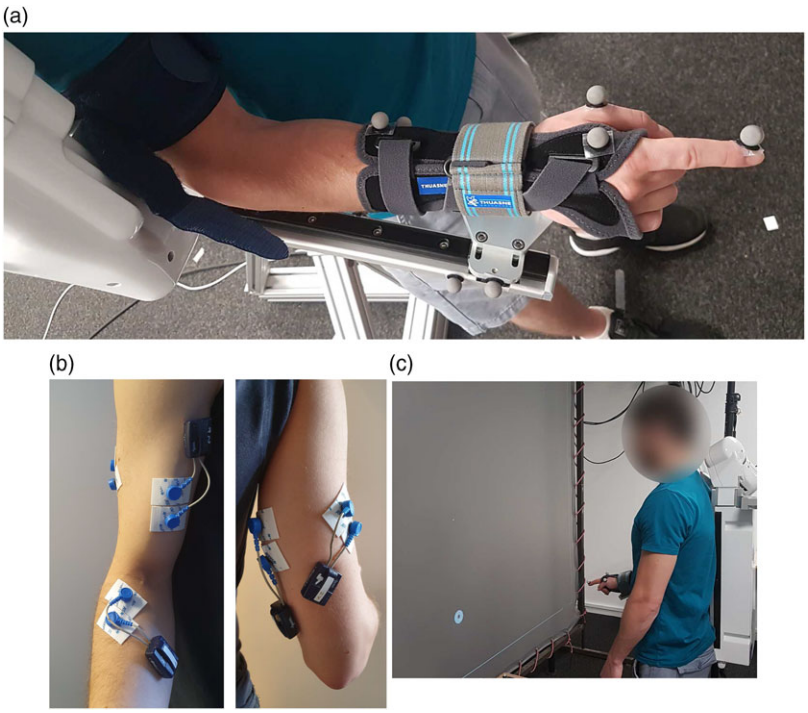

Fig. 4. Description of the experimental setup. (a) Markers on the forearms (human and robot). (b) EMGs on the human arm. (c) Target pointing example.

illustrated in Fig. 4(a). Two markers are placed on the index in order to compute the index direction and three markers are placed on the splint in order to compute the forearm direction. A total of eight infrared cameras are placed around the robot. During the experiment, the evolution of the angular position of the human elbow and the evolution of the angular position of the robot elbow are tracked respectively by the motion capture device and the incremental encoder of the robot. Four electromyographs (EMG) (Cometa, Wave Plus wireless EMG system, Rue de Laval, 53210 Soulgé-sur-Ouette) are placed on the participants as described in Fig. 4(b). The activity of two elbow flexor muscles (biceps brachial and brachioradialis) and two elbow extensor muscles (triceps brachial lateral head and triceps brachial long head) is recorded. The location of the EMG sensors follows the SENIAM recommendations.[47]

Task. The task consisted of point-to-point reaching movements in the sagittal plane involving elbow flexion–extension only. Goals are displayed as targets on a large screen in front of participants as described in Fig. 4(c). A pointer representing the human index forearm line projection is also displayed in real time. Participants are asked to position and keep the pointer on the target location for around 2 s. Once this condition is satisfied, the current target disappears and a new target is displayed. The 0 degree reference is 30 degrees below the horizontal. Five amplitudes of movements are imposed: 12, 24, 36, 48 and 60 degrees rotations around the elbow axis. Movements are performed under four different conditions. Both conditions and amplitudes are randomised accross participants. For each condition, trials consisted of 10 upward and 10 downward movements per amplitude, resulting in 400 movements per participant in total. Participants take a 2 min pause every 50 movements. Two sets of movements are thus performed per condition. One control condition is carried out without ABLE and the three others with ABLE, involving different control laws (details are given in Section 4.2). The participants are standing straight, their back leaning against the rigid base of the exoskeleton. In case of movements performed with ABLE, the right forearm is attached to the robotic device as described in Fig. 4(a). The participant is wearing a splint to ensure the wrist immobilisation and improve interaction via a contact area augmentation.[14]

https://doi.org/10.1017/S0263574720001459 Published online by Cambridge University Press

4.2. Transparent laws implemented

Three control laws are implemented. The first law is a closed-loop position control and the second and third laws are open-loop controls purely based on compensations of the dynamic model developed in Eq. (3). In the second law, the friction compensation is not taken into account in order to test the effect of an incomplete identification. Only the third law includes a complete compensation of the dynamic model of the last joint of ABLE given in Eq. (3). These choices are made to ensure that very different levels of transparency are compared during the experimentations.

The first implemented law is a closed-loop position control developed by the constructor (named CLPC in the rest of this paper). The position control is combined with a partial identification of the robot including the Coulomb friction and the gravity torque compensations. The other parameters of the dynamic model are not taken into account, in particular, there are no compensation of the viscous friction, no compensation of the inertia and no difference of compensation between upward and downward movements. This law is used as a representative of basic identifications, without dependency on movement direction, coupled to closed-loop control to compensate model error. Furthermore, the position control is achieved by estimating the next position of the robot based on the current estimation of the velocity derived from encoder positions and the sampling frequency of the control panel (1 kHz). The estimation of velocity derived from encoders is known to be problematic, particularly for low velocities as described in ref. [48], and could therefore lead to a decrease in transparency near movement initiation. This law is used as a basis for augmented reality tasks by the constructor and provides a first level of transparency. A difference in experimental conditions between the experimentations with this law and with the other conditions is the reference position of the robot that could not be locked for this control law because the implementation provided by the constructor does not allow to mix a classic position control for the shoulder and a transparent control for the elbow. In order to reduce the bias linked to this behaviour, the robot is manually maintained in position during the experimentation. This bias is in favour of this law for the comparison because of its tendency to decrease the overall rigidity of the system, and therefore allow small unwanted movements of the participants.

The two other laws rely on pure compensation of the dynamic model of the elbow of the robot. There is no feedback loop to ensure that the efforts estimated by the identified model are consistent with the input of the user like for the CLPC law and its position feedback. In this sense, these laws can be qualified of open loop. They are based on the results of the identification process (see Section 3), one taking into account the friction law identified to compensate its effects (named FC as Full Compensation) and one not compensating friction (named PCFr as Partial Compensation without Friction). For these two laws, the reference position of the upper arm is locked thanks to a position control of the shoulder based on position measurements and a PI correction to avoid static errors. The full compensation of the inertia is not possible without anticipating the compensation thanks to feedforward architectures.[42] Moreover, obtaining a correct estimation of the acceleration derived from the discrete positions of the encoders can be very complicated, particularly for low velocities. Therefore, a control law simulating the inertial effects is applied directly on the velocity, this law is described in Eq. (8):

$$\hat{M}(x, \dot{q}_{meas}) = J_{eq}(x)\dot{q}_{meas}^{k}, \tag{8}$$

where $\hat{M}(x, \dot{q}_{meas})$ is the estimated inertia torque appearing in blue in Fig. 5, $J_{eq}(x)$ is the identified inertia of the last joint, $\dot{q}_{meas}$ is the articular velocity of the robot derived from position measures, x is the slider position and k is a tuning parameter whose average value is based on participants' sensitivity. For upward movements, the value $k = -1$ is chosen whereas for downward movements, the value providing best results is $k = -1.9$. Preliminary tests, involving five participants different from the main experiment, were performed to adjust the value of k. The tuning was based on subjective feelings reported by the tested participants in an attempt to minimise shaking and resistance to movement. Participants of the main experiment reported no discomfort, blockage or vibration with this tuning. The law presented in Eq. (8) tends to increase the motor current at low velocities to overcome the inertia and to decrease the motor currents linked to inertia at high velocities when accelerations of the human movements are minimal (see Fig. 6). The control schemes implemented for the different conditions of the experiment are described in Fig. 5.

https://doi.org/10.1017/S0263574720001459 Published online by Cambridge University Press

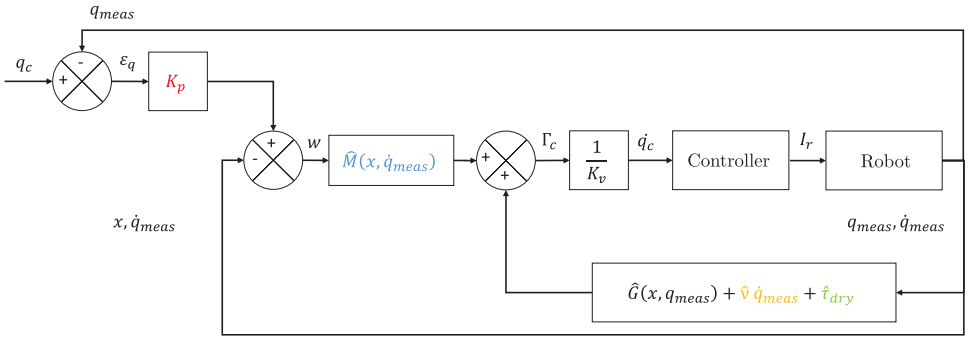

Fig. 5. Control schemes of ABLE implemented. Red: $K_p = 0$ for the FC and PCFr laws. Blue: $\hat{M}(x, \dot{q}_{meas}) = 1$ for the CLPC law. Orange: $\hat{\nu} \neq 0$ for the FC law. Green: $\tau_{dry} = 0$ for the PCFr law.

4.3. Data processing

The angular position of the human elbow is computed as the angle of the forearm made with the vertical. Angular velocity and acceleration are obtained by numerical differentiation of the low-pass filtered (*fourth*-order Butterworth, 3 Hz cut-off frequency) angular elbow position. The start and end of the effective movements are identified as the first and last frame, when the elbow angular velocity is above 5% of maximum velocity. The movement duration is simply computed as the time difference between the first and last frame of the movement. EMGs' signals are filtered using a bandpass filter (*fourth*-order Butterworth, [20, 450] Hz cut-off frequency), centred and rectified.[49] For each subject and each muscle, EMG signals are normalised by the maximal activity reached during the experiment. EMGs signals start and end are advanced of 0.1 s compared to kinematic signals because of the electromechanical delay[50] and to better capture the EMGs burst that causes the instantaneous acceleration.

4.4. Transparency assessment

The transparency of the laws presented in Section 4.2 must be assessed in order to determine the influence of the identification process. As a consequence, the impact of the implemented laws needs to be evaluated on the basis of pre-existing indices.[10] These indices are based on global kinematic characteristics of one movement, whether based on the duration of the movement, on the symmetry of the velocity profile and on its smoothness.

Overall kinematics. The pointing task performed by the participants has been accomplished without velocity or duration constraints. As previously observed,[22] typical unrestrained arm reaching movements are characterised by bell-shaped velocity profiles. Then, basic movement parameters such as movement duration and maximal velocity are a first relevant description of the motion kinematics. It is known that individuals have a preferred movement pace which may be optimally determined by a trade-off between energy and time costs.[51] Furthermore, movement duration and maximal velocity are both known to increase with the amplitude of movement. Affine fits capture quite well these dependencies. The fact that movement velocity increases with amplitude to limit the associated increase in movement time is sometimes referred to as the isochrony principle (although there is no exact isochrony).[52] It has been shown that the wearing of a "transparent" exoskeleton tends to slow down the movement whatever the amplitude.[9] Therefore, we assume that simple indices such has movement duration and maximal velocity are relevant for a macroscopic approach in order to assess the transparency of the tested control laws and their effects on human movement kinematics. We also assume that the conservation of the "isochrony" principle (i.e., approximately affine relationships between amplitude and duration or velocity) is necessary to deem a control law as "transparent".

Muscle activation-based index. None of the previous indices can assess the link between motor command and the resulting acceleration of the human forearm even though it is a critical point to assess the transparency. Indeed, it is important to know how the wearing of the exoskeleton impacts the ratio conversion between these two variables. It has been shown that a high correlation exists between acceleration duration phase and agonist muscle burst duration for forearm flexion and extension.[53] Furthermore, the amount of activation during the two agonist muscle bursts involved in a typical

https://doi.org/10.1017/S0263574720001459 Published online by Cambridge University Press

Table III. Results obtained on movement durations. Ctrl: Control condition without wearing the exoskeleton. FC: Full compensation based on identification. PCFr: Partial Compensation based on identification without Friction compensation. CLPC: Closed-loop position control.

Condition	Mean duration (s)	Standard deviation (s)	Min (s)	Median (s)	Max (s)
Ctrl	0.957	0.199	0.782	0.870	1.281
FC	0.980	0.203	0.793	0.900	1.271
PCFr	1.150	0.260	0.829	1.065	1.520
CLPC	1.135	0.283	0.834	1.060	1.494

triphasic-pattern is also correlated with the acceleration of a rapid movement.[54] In addition, the maximal acceleration is a good indicator of the movement plan because motor corrections from sensory feedback have little time to come into play. An EMG-based transparency index is thus defined as the ratio between the agonists Root Mean Square (RMS) activation and the maximal acceleration during the movement phase. We then subtracted and normalised the obtained value with the control condition value (without exoskeleton). A value equal to zero reflects that the RMS activation of agonists muscles create the same acceleration than without exoskeleton. This index is called "EMG/Acc" and reflects the muscle activation yield. This index may provide useful information because it integrates measures that participate in the initialisation of the movement and, therefore, are good indicators of the planning of the movement operated by the participants and of the potential perturbation induced by the exoskeleton. As previously shown,[55,56] the planning of the movement is strongly influenced by exterior perturbations that are internally modelled by humans such as, in this case, an exoskeleton. Therefore, this index reflects how hard the participants expect the movement to be. The expression of this index is given in Eq. (9):

$$EMG/Acc = \frac{1}{C}\left(\frac{A_{agonist,RMS}}{\ddot{q}_{elbow,\max}}\right) - 1, \tag{9}$$

where $A_{agonist,RMS}$ is the mean RMS activation of the agonist muscles (here the biceps and brachioradialis), $\ddot{q}_{elbow,\max}$ is the maximal angular acceleration of the elbow and $C = A_{agonist,RMS}/\ddot{q}_{elbow,\max}$ is the ratio obtained with the control condition (without exoskeleton). This index is not computed for downward movements because of the gravity working in the same direction as the agonists muscle (i.e., triceps brachial lateral head and triceps brachial long head). Indeed, the extensors activation is not solely responsible of the movement. An inactivation of antigravity muscles is observed initially to accelerate a downward movement.[57] Observed bursts were too weak to get exploitable data for these downward movements executed at a self-selected velocity (but this could be circumvented in future studies by asking participants to move faster).

4.5. Statistical analysis

Descriptive and inferential statistical analyses are performed on the participants' mean values so that the resulting variability is between participants. The Friedman non-parametric statistical test is performed with studied control laws as the factor. This test gives an estimated χ^2 score which allows to obtain a p-value from a χ^2 table. *Post hoc* comparisons are conducted using the Nemenyi test. This is a conservative test allowing pairwise comparisons. Both Friedman and Nemenyi statistical tests are performed using the PMCMR R package.[58] The Nemenyi test is performed separately for upward and downward movement directions in case of the relative duration to maximum velocity. For the "*EMG/Acc*" index, analyses are performed only for upward movements for reasons explained in Section 4.4. For all indices, the tests are carried out on the average values over the amplitudes. For all tests the level of significance is fixed at $p < 0.05$.

5. Results and Discussion

Overall kinematics. The first observation that can be done is that the global profile of vertical arm movements previously observed[22] is preserved when wearing an exoskeleton. Indeed, the bell-shaped velocity profiles are present and the trajectories and acceleration profiles are similar, as exemplified

https://doi.org/10.1017/S0263574720001459 Published online by Cambridge University Press

Table IV. Results obtained on movements maximal velocity. Ctrl: Control condition without wearing the exoskeleton. FC: Full compensation based on identification. PCFr: Partial Compensation based on identification without Friction compensation. CLPC: Closed-loop position control.

Condition	Mean max velocity (rad.s^{-1})	Standard deviation (rad.s^{-1})	Min (rad.s^{-1})	Median (rad.s^{-1})	Max (rad.s^{-1})
Ctrl	1.416	0.326	0.928	1.526	1.770
FC	1.345	0.255	0.967	1.413	1.655
PCFr	1.145	0.301	0.774	1.181	1.610
CLPC	1.116	0.191	0.776	1.110	1.518

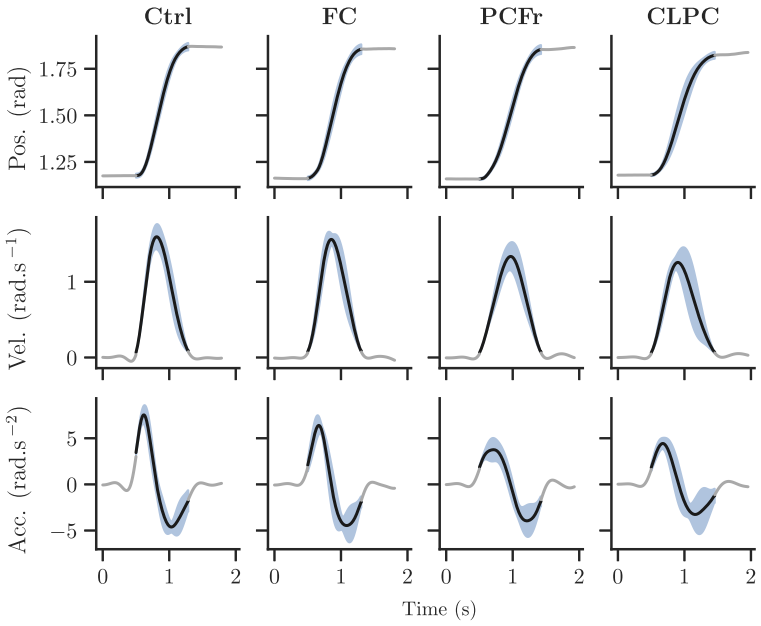

Fig. 6. Averaged position, velocity and acceleration on upward 36° movements for one participant. Ctrl: Control condition without wearing the exoskeleton. FC: Full Compensation based on identification. PCFr: Partial Compensation based on identification without Friction compensation. CLPC: Closed-loop position control.

in Fig. 6. Then, as detailed in Section 4.4, the average durations of all movements (all amplitudes and participants pooled together) is tested through the control laws. These mean durations are reported together with standard deviation, minimum and maximum values and median in Table III. At first sight, the FC law seems to affect the execution duration and its standard deviation less than the other two laws.

This main observation is confirmed by a statistical analysis. Statistical differences were observed on movement duration data ($\chi^2 = 14.4$, $p = 0.002$). The pairwise comparison showed no significant difference between the Ctrl and the FC laws. Nevertheless, statistical differences appeared between the Ctrl and the two other laws, for these two laws the result is $p = 0.037$. The same statistical differences (i.e., $p = 0.37$) appeared between the FC law and these two laws. The conclusion given by this statistical analysis is that, in terms of movement execution durations, the FC law has no significant impact contrary to the PCFr and CLPC laws. This result confirms that, as previously introduced,[10] the duration of the whole movement can be a good first-sight performance index to estimate the achieved level of transparency.

The second pre-existing performance index that can be used to evaluate transparency is the conservation of the maximum velocity of the participants. The results obtained with the different laws are compiled in Table IV.

https://doi.org/10.1017/S0263574720001459 Published online by Cambridge University Press

Table V. Descriptive statistics of the obtained coefficients of determination (R^2) for regression analyses on amplitude and mean velocity relationships. Ctrl: Control condition without wearing the exoskeleton. FC: Full compensation based on identification. PCFr: Partial Compensation based on identification without Friction compensation. CLPC: Closed-loop position control.

Condition	Direction	R^2	Standard deviation	Min	Median	Max
Ctrl	Up	0.972	0.028	0.930	0.990	0.997
	Down	0.949	0.052	0.873	0.977	0.991
FC	Up	0.942	0.054	0.846	0.957	0.986
	Down	0.938	0.037	0.884	0.948	0.982
PCFr	Up	0.963	0.018	0.927	0.967	0.979
	Down	0.968	0.034	0.912	0.985	0.995
CLPC	Up	0.961	0.040	0.892	0.971	0.997
	Down	0.953	0.046	0.895	0.972	0.997

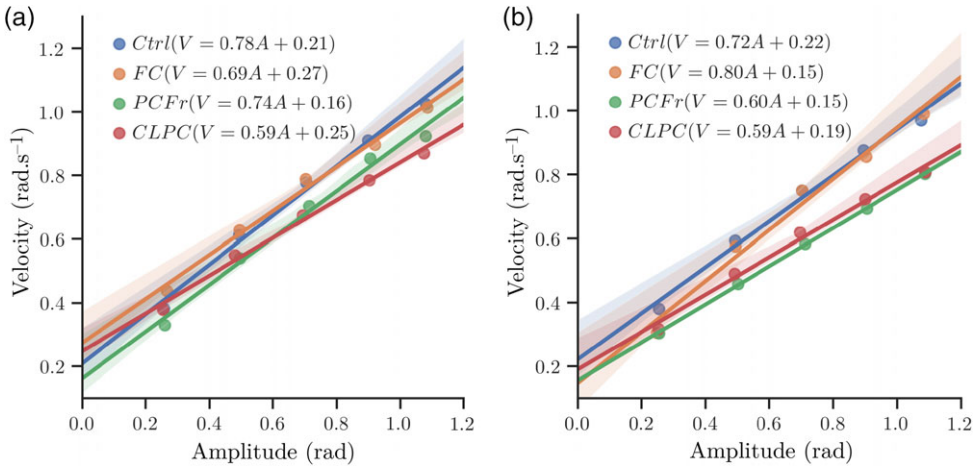

Fig. 7. Isochrony principle verification for the different conditions. Equations of affine functions are given with V the mean velocity and A the amplitude. Ctrl: Control condition without wearing the exoskeleton. FC: Full Compensation based on identification. PCFr: Partial Compensation based on identification without Friction compensation. CLPC: Closed-loop position control. (a) Upward movements. (b) Downward movements.

The Friedman test is significant ($\chi^2 = 15.4$, $p = 0.015$) which means that statistical differences were observed on the movement maximal velocity data. The pairwise comparison showed no statistical difference between the Ctrl and the FC laws ($p = 0.808$). Furthermore, statistical differences appeared between the Ctrl and the two other laws. The result is $p = 0.019$ for the PCFr law and $p = 0.004$ for the CLPC law. No statistical difference is observed between FC and PCFr laws (i.e., $p = 0.183$) and between FC and CLPC laws ($p = 0.066$). Finally, according to this index, the FC law has a lower impact on the human movement than the two other laws because there is no significant difference between this condition and the Ctrl condition as opposed to the PCFr and CLPC conditions.

The third kinematic index that can be tested is the conservation of the isochrony principle. If this index is not verified, the tested control law cannot be qualified as transparent because it would imply that the movement cannot be seen as unrestrained, which is the objective of a transparent law.

Despite differences in movement velocity across control laws, the affine relation between amplitude and mean velocity is preserved (see Fig. 7). As can be seen in Table V, participants averaged relationships are strong and coefficients of determination (R^2) are comparable to those obtained in the motor control literature.[59] Hence, even if there are some minor differences on the slopes and intercepts across conditions it is important to note that this fundamental human movement feature is still present with the three control laws.

https://doi.org/10.1017/S0263574720001459 Published online by Cambridge University Press

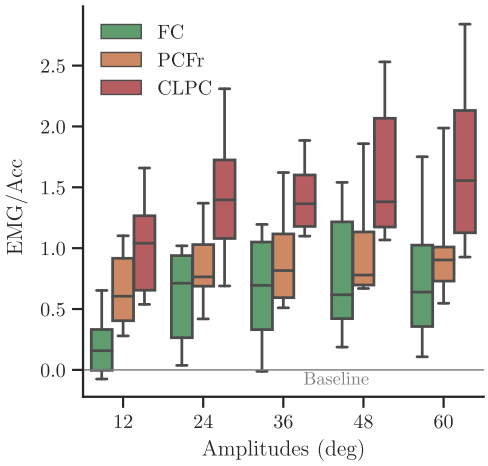

Fig. 8. Agonist muscle transparency index for the different conditions and for upward movements. FC: Full Compensation based on identification. PCFr: Partial Compensation based on identification without Friction compensation. CLPC: Closed-loop position control.

Conclusion on pre-existing indices. Overall, we can conclude that the three implemented laws can be qualified of transparent because they preserve the isochrony principle and the overall shapes of the position, velocity and acceleration profiles. For the FC law, neither the mean duration nor the mean maximal velocity of movement are significantly different from the Ctrl law which is not verified for the other two laws. Therefore, the FC law appears to be the most transparent according to global conservation of the kinematic characteristics related to the velocity of the human movement.

EMG/Acc index. The new index introduced in this paper, described in Section 4.4, is the "*EMG/Acc*" index. This index is computed on the data retrieved during the experimentations and the results are available in Fig. 8.

The mean results displayed in Fig. 8 show an improvement of the muscular activation/acceleration yield with the use of the FC law compared to the two other laws. The CLPC law seems to be the least transparent according to the *EMG/Acc* index. In order to confirm these observations, the same statistical analysis as previously has been conducted. The Friedman test showed significant differences between the conditions ($\chi^2 = 12$, $p = 0.002$) and the pairwise comparison *post hoc* showed a significant difference between the FC law and the CLPC law ($p = 0.001$). The statistical difference between the FC law and the PCFr law is not proven by the available dataset ($p = 0.193$). These results show that with the FC law, participants are more likely to produce a greater acceleration with the same amount of muscular activation than with the CLPC law. This supports the fact that the *EMG/Acc* index can be used to express the level of transparency of a law because it shows quantifiable differences between the different conditions, in the same trend of pre-existing indices. This also confirms that the implemented FC law gives a better level of transparency than the other two laws on average and than the CLPC law via a statistical analysis.

6. Conclusion

The first aim of this study was to improve the transparency of a powered upper limb exoskeleton.[27] The transparency at the elbow axis level is enhanced by using a direction-dependent model for identification inspired by the direction-dependent friction model previously introduced[32] and by using a control law trying to compensate the whole dynamic of the exoskeleton forearm. Then, we evaluated the behaviour of our new control law on six participants and compared it to the behaviour of two other laws and to the behaviour of participants without the exoskeleton. We also made sure that the behaviours obtained on upward and downward motions followed the same trends and, therefore, confirmed the consistency of our identification procedure. Our results on pre-existing indices show that an accurate identification is a significant step towards a better transparency of exoskeletons. Moreover, the approach based on a dissociation of the identified models for upward and downward movements could be beneficial for this type of devices. Indeed, in order to be usable in the medical or industrial fields, exoskeletons need to reach high levels of backdriveability that can only be achieved

https://doi.org/10.1017/S0263574720001459 Published online by Cambridge University Press

by reducing the overall rigidity and precision of the internal guidances. In this paper, we showed that this drawback can be mitigated by this a relatively advanced identification.

The second objective of this study was to introduce a new performance index to evaluate transparency. This index is based on the ratio between agonist muscle activation (measured by EMG) and peak acceleration of the human limb after movement initiation. It takes the form of a normalised ratio of these two features of the human movement and is called *EMG/Acc*. This index showed significant differences between two of the different implemented transparent control laws. As the results followed the same trend as those obtained with pre-existing indices, this index may be a relevant indicator of transparency. The main advantage of this index is to assess the level of transparency with regard to the efficiency of the conversion between muscle activity and peak acceleration, as well as the effects of wearing an exoskeleton. Therefore, this index is relevant in both industrial and medical applications. Furthermore, this index could be used in any one-degree-of-freedom task to validate or study different types of laws, such as transparent or assistive laws. Nevertheless, the generalisation to n degrees of freedom seems to be complex as the treatment of EMG of n agonists muscles acting simultaneously can be very challenging.

As closed-loop position-based control laws have shown limited capacities in terms of improving the level of transparency, future studies will be conducted after the implementation of a force sensor at the level of the wrist. This force sensor will allow the quantification of the interaction efforts and the development of a closed-loop control law based on its measurements that should improve the level of transparency further. Another measure that could be included is EMG which could lead to a predictive control law, anticipating the direction and the starting force of the movement. This transparent law would then be used as a basis to study the human motor control when wearing an exoskeleton.

Acknowledgements

We thank F. Geffard and P. Garrec for meaningful discussions. This work is supported by the "IDI 2017" project funded by the IDEX Paris-Saclay, ANR-11-IDEX-0003-02. This work is supported by the French National Agency for Research (grant ANR-19-CE33-0009).

References

1. W. Huo, V. Arnez-Paniagua, G. Ding, Y. Amirat and M. Samer, "Adaptive proxy-based controller of an active ankle foot orthosis to assist lower limb movements of paretic patients," *Robotica* **37**(12), 2147–2164 (2019).
2. R. Bogue, "Robotic exoskeletons: A review of recent progress," *Ind. Robot Int. J.* **42**(1), 5–10 (2015).
3. M. P. de Looze, T. Bosch, F. Krause, K. S. Stadler and L. W. O'Sullivan, "Exoskeletons for industrial application and their potential effects on physical work load," *Ergonomics* **59**(5), 671–681 (2016).
4. A. Frisoli, C. Procopio, C. Chisari, I. Creatini, L. Bonfiglio, M. Bergamasco, B. Rossi and M. C. Carboncini, "Positive effects of robotic exoskeleton training of upper limb reaching movements after stroke," *J. Neuroeng. Rehabilit.* **9**(1), 36 (2012).
5. A. Frisoli, L. Borelli, A. Montagner, S. Marcheschi, C. Procopio, F. Salsedo, M. Bergamasco, M. C. Carboncini, M. Tolaini and B. Rossi, "Arm Rehabilitation with a Robotic Exoskeleleton in Virtual Reality," *IEEE 10th International Conference on Rehabilitation Robotics, 2007. ICORR 2007* (IEEE, 2007) pp. 631–642.
6. N. Sylla, V. Bonnet, F. Colledani and P. Fraisse, "Ergonomic contribution of ABLE exoskeleton in automotive industry," *Int. J. Ind. Ergon.* **44**(4), 475–481 (2014).
7. L. M. Mooney, E. J. Rouse and H. M. Herr, "Autonomous exoskeleton reduces metabolic cost of human walking during load carriage," *J. NeuroEng. Rehabil.* **11**(1), 80 (2014).
8. J. M. Veerbeek, A. C. Langbroek-Amersfoort, E. E. van Wegen, C. G. Meskers and G. Kwakkel, "Effects of robot-assisted therapy for the upper limb after stroke: A systematic review and meta-analysis," *Neurorehabil. Neural Repair* **31**(2), 107–121 (2017).
9. S. Bastide, N. Vignais, F. Geffard and B. Berret, "Interacting with a 'Transparent' Upper-Limb Exoskeleton: A Human Motor Control Approach," *IEEE/RSJ International Conference on Intelligent Robots and Systems (IROS)* (2018) pp. 4661–4666.
10. N. Jarrassé, M. Tagliabue, J. V. G. Robertson, A. Maiza, V. Crocher, A. Roby-Brami and G. Morel, "A methodology to quantify alterations in human upper limb movement during co-manipulation with an exoskeleton," *IEEE Trans. Neural Syst. Rehabil. Eng.* **18**(4), 389–397 (2010).
11. C. Di Natali, T. Poliero, M. Sposito, E. Graf, C. Bauer, C. Pauli, E. Bottenberg, A. De Eyto, L. O'Sullivan, A. F. Hidalgo, D. Scherly, K. S. Stadler, D. G. Caldwell and O. Jess, "Design and evaluation of a soft assistive lower limb exoskeleton," *Robotica* **37**, 1–21 (2019).

12. G. Ercolini, E. Trigili, A. Baldoni Simona Crea and N. Vitiello, "A novel generation of ergonomic upper-limb wearable robots: Design challenges and solutions," *Robotica* **37** (12,SI), 2056–2072 (2018).
13. V. S. Huang and J. W. Krakauer, "Robotic neurorehabilitation: A computational motor learning perspective," *J. NeuroEng. Rehabil.* **6**(5), 1–13 (2009).
14. N. Jarrassé and G. Morel, "Connecting a human limb to an exoskeleton," *IEEE Trans. Robot.* **28**(3), 697–709 (2012).
15. X. Jin, Y. Cai, A. Prado and S. K. Agrawal, "Effects of Exoskeleton Weight and Inertia on Human Walking," *2017 IEEE International Conference on Robotics and Automation (ICRA)* (IEEE, Singapore, 2017) pp. 1772–1777.
16. D. Martelli, F. Vannetti, M. Cortese, P. Tropea, G. Francesco, S. Micera, V. Monaco and N. Vitiello, "The effects on biomechanics of walking and balance recovery in a novel pelvis exoskeleton during zero-torque control," *Robotica* **32**(08), 1317–1330 (2014).
17. M. Xiloyannis, D. Chiaradia, A. Frisoli and L. Masia, "Physiological and kinematic effects of a soft exosuit on arm movements," *J. NeuroEng. Rehabilit.* **16**(1), 29 (2019).
18. T. Proietti, V. Crocher, A. Roby-Brami and N. Jarrasse, "Upper-limb robotic exoskeletons for neurorehabilitation: A review on control strategies," *IEEE Rev. Biomed. Eng.* **9**, 4–14 (2016).
19. N. Jarrassé, J. Paik, V. Pasqui and G. Morel, "How can Human Motion Prediction Increase Transparency?," *IEEE International Conference on Robotics and Automation* (2008) pp. 2134–2139.
20. A. Ajoudani, A. M. Zanchettin, S. Ivaldi, A. Albu-Schäffer, K. Kosuge and O. Khatib, "Progress and prospects of the human-robot collaboration," *Auto. Robots* **42**, 957–975 (2017).
21. E. Pirondini, M. Coscia, S. Marcheschi, G. Roas, F. Salsedo, A. Frisoli, M. Bergamasco and S. Micera, "Evaluation of the effects of the Arm Light Exoskeleton on movement execution and muscle activities: A pilot study on healthy subjects," *J. NeuroEng. Rehabil.* **13**, (2016), Article 9.
22. C. G. Atkeson and J. M. Hollerbach, "Kinematic features of unrestrained vertical arm movements," *J. Neurosci.* **5**(9), 2318–2330 (1985).
23. J. Gaveau, B. Berret, L. Demougeot, L. Fadiga, T. Pozzo and C. Papaxanthis, "Energy-related optimal control accounts for gravitational load: comparing shoulder, elbow, and wrist rotations," *J. Neurophysiol.* **111** (1), 4–16 (2014).
24. T. Flash and N. Hogan, "The coordination of arm movements: An experimentally confirmed mathematical model," *J. Neurosci.* **5**(7), 1688–1703 (1985).
25. P. Morasso, "Spatial control of arm movements," *Exp. Brain Res.* **42**(2), 223–227 (1981).
26. P. Garrec, "Screw and Cable Acutators (SCS) and Their Applications to Force Feedback Teleoperation, Exoskeleton and Anthropomorphic Robotics," **In:** *Robotics 2010 Current and Future Challenges* (2010) pp. 167–191.
27. P. Garrec, J. P. Friconneau, Y. Méasson and Y. Perrot, "ABLE, an Innovative Transparent Exoskeleton for the Upper-Limb," *IEEE/RSJ International Conference on Intelligent Robots and Systems (IROS)* (2008) pp. 1483–1488.
28. R. Mallat, M. Khalil, G. Venture, V. Bonnet and S. Mohammed, "Human-Exoskeleton Joint Misalignment: A Systematic Review," In *2019 Fifth International Conference on Advances in Biomedical Engineering (ICABME)* (IEEE, 2019).
29. A. Schiele and F. C. T. van der Helm, "Kinematic design to improve ergonomics in human machine interaction," *IEEE Trans. Neural Syst. Rehabil. Eng.* **14**(4), 456–469 (2006).
30. L. Peternel, T. Noda, T. Petrič, A. Ude, J. Morimoto and J. Babič, "Adaptive control of exoskeleton robots for periodic assistive behaviours based on EMG feedback minimisation," *PLOS ONE* **11**(2), e0148942, 1–26 (2016).
31. C. Carignan, J. Tang and S. Roderick, "Development of an Exoskeleton Haptic Interface for Virtual Task Training," *2009 IEEE/RSJ International Conference on Intelligent Robots and Systems* (IEEE, 2009).
32. P. Hamon, M. Gautier and P. Garrec, "Dynamic Identification of Robots with a Dry Friction Model Depending on Load and Velocity," *IEEE/RSJ International Conference on Intelligent Robots and Systems (IROS)* (2010) pp. 6187–6193.
33. M. Franken, S. Stramigioli, R. Reilink, C. Secchi and A. Macchelli, "Bridging the gap between passivity and transparency," *Robot. Sci. Syst. V* **36**, 36–44 (2009).
34. W. Khalil and E. Dombre, *Modélisation, identification et commande des robot* (2003).
35. S. Moberg, Modeling and Control of Flexible Manipulators *Ph.D. Thesis* (Linkping University, 2010).
36. M. Östring, S. Gunnarsson and M. Norrlöf, "Closed-loop identification of an industrial robot containing flexibilities," *Control Eng. Practice* **11**(3), 291–300 (2003).
37. L. Ljung, *System Identification: Theory for the User* (Prentice Hall PTR, Upper Saddle River, New Jersey, 1999).
38. C. Gong, J. Yuan and J. Ni, "Nongeometric error identification and compensation for robotic system by inverse calibration," *Int. J. Mach. Tools Manuf.* **40**(14), 2119–2137 (2000).
39. S. Hayati and M. Mirmirani, "Improving the absolute positioning accuracy of robot manipulators," *J. Robot. Syst.* **2**(4), 397–413 (1985).
40. J.-M. Renders, R. Hanus and E. Rossignol, "Kinematic calibration and geometrical parameter identification for robots," *IEEE Trans. Robot. Autom.* **7**, 721–732 (1992).
41. M. Gautier, "Dynamic Identification of Robots with Power Model," *Proceedings of the 1997 IEEE International Conference on Robotics and Automation* (1997) pp. 1922–1927.

https://doi.org/10.1017/S0263574720001459 Published online by Cambridge University Press

42. F. Geffard, C. Andriot, A. Micaelli and G. Morel, "On the Use of a Base Force/Torque Sensor in Teleoperation," *IEEE International Conference on Robotics and Automation* (2000) pp. 2677–2683.
43. M. Gäfvert, P. Lischinsky, H. Olsson, K. J. Åström and C. Canudas de Wit, "Friction models and friction compensation," *Eur. J. Control* **4**(176), 176–195 (1998).
44. M. T. Pham, M. Gautier and P. Poignet, "Identification of Joint Stiffness with Bandpass Filtering," *IEEE International Conference on Robotics and Automation* (2001) pp. 2867–2872.
45. N. D. Vuong and M. H. Ang, Jr., Dynamic model identification for industrial robots. *Acta Polytechnica Hungarica* **6**(5), 51–68 (2009).
46. World Medical Association, "World Medical Association Declaration of Helsinki. Ethical principles for medical research involving human subjects," *Bull. World Health Organizat.* **79**(4), 373–374 (2001).
47. H. J. Hermens, B. Freriks, C. Disselhorst-Klug and G. Rau, eds., *European recommendations for surface ElectroMyoGraphy: Results of the SENIAM project*, SENIAM, vol. 8 (Roessingh Research and Development, Enschede, 1999).
48. G. Liu, "On Velocity Estimation Using Position Measurements," *Proceedings of the American Control Conference* (2002) pp. 1115–1120.
49. J. Potvin, and S. Brown, "Less is more: High pass filtering, to remove up to 99% of the surface EMG signal power, improves EMG-based biceps brachii muscle force estimates," *J. Electromyography Kinesiol.* **14**(3), 389–399 (2004).
50. P. R. Cavanagh and P. V. Komi, "Electromechanical delay in human skeletal muscle under concentric and eccentric contractions," *Eur. J. Appl. Physiol. Occupat. Physiol.* **42**(3), 159–163 (1979).
51. B. Berret and F. Jean, "Why don't we move slower? The value of time in the neural control of action," *J. Neurosci.* **36**(4), 1056–1070 (2016).
52. P. Viviani and C. Terzuolo, "Trajectory determines movement dynamics," *Neuroscience* **7**(2), 431–437 (1982).
53. J. Cooke and S. Brown, "Movement-related phasic muscle activation: III. The duration of phasic agonist activity initiating movement," *Exp. Brain Res.* **99**(3), 473–482 (1994).
54. J. D. Cooke and S. H. Brown, "Movement-related phasic muscle activation. II. Generation and functional role of the triphasic pattern," *J. Neurophysiol.* **63**(3), 465–472 (1990).
55. J. N. Ingram, I. S. Howard, J. R. Flanagan and D. M. Wolpert, "A single-rate context-dependent learning process underlies rapid adaptation to familiar object dynamics," *PLoS Comput. Biol.* **7**(9) (2011).
56. R. Shadmehr and F. A. Mussa-lvaldi, "Adaptive representation of dynamics during learning of a motor task," *J. Neurosci.* **14**(5), 3208–3224 (1994).
57. J. Gaveau, S. Grospretre, D. Angelaki and C. Papaxanthis, "A cross-species neural integration of gravity for motor optimisation," bioRxiv (2019), 728857.
58. T. Pohlert, The Pairwise Multiple Comparison of Mean Ranks Package (PMCMR). R-Package (2016) pp. 14–19.
59. B. Berret, C. Castanier, S. Bastide and T. Deroche, "Vigour of self-paced reaching movement: Cost of time and individual traits," *Sci. Rep.* **8**(1), 10655–10669, (2018).